Available online at www.sciencedirect.com
ScienceDirect
International Journal of Thermal Sciences 47 (2008) 1359–1373
International Journal of Thermal Sciences
www.elsevier.com/locate/ijts

Effect of geometric parameters on steady-state performance of single-phase NCL with heat loss to ambient

Dipankar Narayan Basu, Souvik Bhattacharyya *, P.K. Das

Department of Mechanical Engineering, Indian Institute of Technology Kharagpur, Kharagpur, India 721302

Received 17 January 2007; received in revised form 23 October 2007; accepted 23 October 2007

Abstract

Present study aims at development of a theoretical model to simulate the steady state performance of a rectangular single-phase natural circulation loop and to investigate the role of different geometric parameters on the system behaviour. The system has been considered as a conjugate problem with interaction of the wall with loop fluid, cooling stream and ambient along different sections of the loop. Non-dimensional form of coupled conservation equations have been solved using 1-d numerical techniques. Predicted values exhibited good degree of agreement with corresponding experimental data from the literature. As NCL is a self-sustaining system and it is difficult to control any flow-related parameters from outside once the system is under operation, it is very much essential to analyze the role of different geometric parameters at design level itself. Detailed parametric variation has been attempted to find operating limits of geometric parameters. Consideration of heat loss to ambient from the loop wall has been found to have significant effect on suitability of system dimensions, particularly under cooler atmospheric conditions. A loop with shorter height and smaller diameter yields higher effectiveness, i.e., transfers larger proportion of input energy to the sink, but employing lower circulation rate due to reduced buoyancy. Longer heating section yields enhanced heat transfer from wall to fluid and has a stabilizing effect on the system. Wall materials with higher thermal conductivity have been found to be more effective to avoid large thermal gradients within the system.

Keywords: Natural circulation; Conjugate problem; Numerical model; Geometry; Steady-state; Effectiveness

1. Introduction

Natural circulation loops (NCLs) provide a very efficient way of transferring heat from a high-temperature source to a low-temperature sink without using any mechanical device. The heat sink is located at an elevation higher than the source. That causes the circulating fluid, heated from bottom and cooled from top, to flow under the influence of gravity, the difference in fluid density between the two vertical arms being the driving force. Highly reliable loop performance and enhanced passive safety due to the absence of any moving parts makes NCL a very lucrative option for source-to-sink heat transfer without bringing them in direct contact. Hence they have found successful application in a number of very important engineering fields, such as, solar heaters, nuclear reactor core cooling, electronic chip cooling, turbine blade cooling, chemical process industries, geothermal energy extraction processes and plenty more [1].

As there is no direct controlling mechanism for NCLs, intense analysis is required to ensure stable zone of operation. Wide applicability and complexity in operation has attracted plenty of research efforts related to NCL and good amount of theoretical and experimental findings are available in literature [1–3]. Pioneering studies of Keller [4] and Welander [5] concluded that loop flow rate is decided by the interplay between friction and buoyancy forces, providing a self-correcting operation, and hence instabilities could occur depending on dynamics of system; a theoretical model of a rectangular loop with point source and sink was presented for explaining the appearance of instabilities in laminar flow situations considering a phase shift between the flow rate and buoyancy force. Zvirin and Greif [6] proposed an approximate method to predict the transient behaviour of the same system; but the method

* Corresponding author. Tel.: +91 3222 282904; fax: +91 3222 255303.
E-mail address: souvik@mech.iitkgp.ernet.in (S. Bhattacharyya).

1290-0729/$ – see front matter
doi:10.1016/j.ijthermalsci.2007.10.010

Nomenclature

A	Area	m^2
C_p	Specific heat	$J\,kg^{-1}\,K^{-1}$
d	Diameter	m
f	Friction factor	
g	Acceleration due to gravity	$m\,s^{-2}$
G	Mass flux	$kg\,m^{-2}\,s^{-1}$
Gr_m	Modified Grashof number	
Gz	Graetz number	
h	Loop height	m
H	Heat transfer coefficient	$W\,m^{-2}\,K^{-1}$
L	Length	m
$\dot{m}$	Mass flow rate	$kg\,s^{-1}$
Nu	Nusselt number	
p	Pressure	$N\,m^{-2}$
Pr	Prandtl number	
$\dot{Q}$	Input power	W
R	Area ratio	
Ra	Rayleigh number	
Re	Reynolds number	
St_m	Modified Stanton number	
t	Time	s
T	Absolute temperature	K
U	Velocity	$m\,s^{-1}$
V	Volume	m^3
W	Loop width	m
z	Length coordinate	m

Greek letters

β	Isobaric volumetric expansion coefficient	K^{-1}
ε	System effectiveness	
λ	Thermal conductivity	$W\,m^{-1}\,K^{-1}$
μ	Dynamic viscosity	$kg\,m^{-1}\,s^{-1}$
θ	Non-dimensional temperature	
ρ	Density	$kg\,m^{-3}$
τ	Non-dimensional time	

Subscripts

0	Reference
a	Ambient
av	Average
c	Cooler
cs	Cross-section
ex	External heat exchanger
f	Loop fluid
h	Heater
in	Inner
out	Outer
ref	Reference
ss	Steady state
tot	Total
w	Wall material

was unable to reconstruct the exact steady state solution. Most of the early experimental and theoretical studies were focused on toroidal configuration [7–10], mainly due of its simplicity in mathematical modelling. Experimental confirmation of the appearance of instability was first presented by Creveling et al. [7]. Different studies have also been reported for U-shaped open loop thermosyphon [11], multiple-path loops [12], figure-of-eight loops [13] etc. Most application areas of single-phase NCL involve a rectangular configuration. Still the amount of available literature related to rectangular NCL is not great in comparison. Bernier and Baliga [14] proposed a 1-d/2-d model of a loop with two vertical legs, connected by two circular 180° bends with vertical heating and cooling, and showed improved results for cases with mixed-convection effects and significance of heat losses through insulations. A 1-d model of a fully rectangular NCL was proposed by Nayak et al. [15] to identify the stable, unstable and neutrally stable conditions by examining flow and temperature oscillations and also through linear stability analysis. Steady state and stability behaviour of a similar configuration was also studied by Vijayan et al. [16,17]. Detailed steady-state performance of a single-phase NCL has been reported by Vijayan et al. [18], where they showed that both friction and heat transfer are affected by the presence of buoyancy-induced flow under steady-state natural circulation condition. A generalized non-loop-specific correlation was proposed to predict hydraulic loss coefficient. Rao et al. [19,20] studied a heat exchanger-coupled closed NCL and following 1-D conservation equations, derived closed form equations to predict the influence of different parameters on loop flow rate.

A meticulous survey of the available literature, however, reflects that most of the reported studies present qualitative predictions. As was suggested by Vijayan [21], in order to have quantitative prediction, it is necessary to consider wall heat conduction effects. Jiang and Shoji [22] considered the effect of wall conduction, assuming identical temperature gradient for the wall and the loop fluid, for a toroidal loop and observed significant effect of wall conductivity on flow stabilization. It is therefore, necessary to consider NCL as a conjugate system, with interaction between wall and loop fluid.

As NCL is a self-sustaining system and it is difficult to control any flow-related parameters from outside once the system is under operation, it is very much essential to analyze the role of different geometric parameters at design level itself. Generally for theoretical studies, the system is assumed to be ideally insulated; which they are not in practice. There is bound to be some heat loss to the ambient, thereby reducing the effective temperature differential between the vertical arms, which can no longer be taken as the difference across the heat-exchanging sections. An earlier study of the present authors had suggested that heat loss can have significant effect on system behavior [23]. It is, therefore, very important to understand the influence of different geometric parameters on system performance, while sub-

jected to heat losses to surrounding. That will help to design the system properly for the expected ranges of parameters corresponding to the specific field of application. For that purpose, present work focuses on development of a numerical model simulating a single-phase rectangular NCL, with the primary objective of studying the effect of various geometric parameters on its static performance, particularly when the system is subjected to heat loss to the ambient.

2. Theoretical modelling

2.1. Physical description of rectangular NCL and assumptions

Fig. 1 shows the geometrical description of the single-phase rectangular NCL under consideration. Buoyancy being the sole driving force, it is necessary to have the thermal source placed below the sink. Here the loop fluid receives a constant power input from an external source (AB) located along the bottom horizontal arm. Cooling of fluid is achieved by a parallel-flow heat exchanger (CD) positioned around the top horizontal arm. The source and sink is considered to be perfectly insulated from the surrounding, which implies that their only mode of thermal interaction is energy transfer with loop wall. However, the vertical arms and uninsulated sections of the horizontal arms (BC and DA) are in thermal contact with atmosphere and are subjected to heat loss to the cooler ambient. Water is considered to be the working fluid, as well as the cooling medium.

A number of justifiable assumptions have been considered to simplify the present mathematical model.

(a) Any variation in the radial direction has been neglected, resulting in a completely 1-d model of NCL. At higher flow rates, fluid is expected to be well mixed at any cross-section, giving a nearly uniform velocity profile with negligible boundary effects and leading to insignificant deviation in the radial direction.

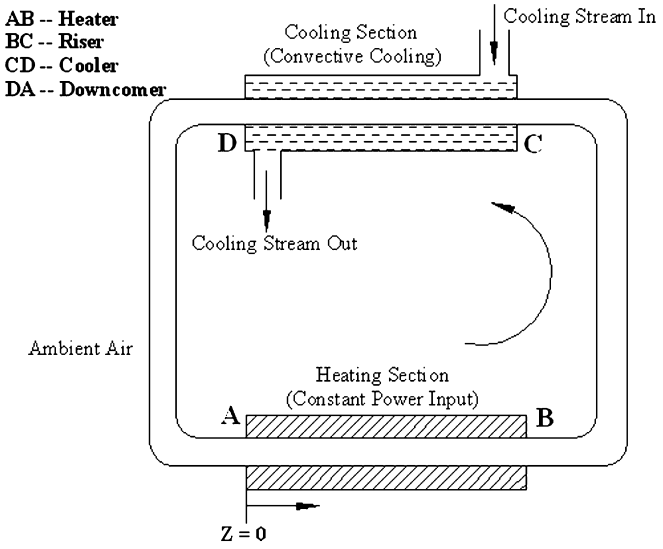

Fig. 1. Geometry of rectangular natural circulation loop (NCL).

(b) Boussinesq approximation is valid, accordingly density variation has been considered only in the body force term of the loop momentum equation.
(c) Negligible pressure loss at the pipe bends.
(d) Viscous dissipation has been neglected in the energy equation.
(e) Constant properties of the wall material.
(f) Vertical flat plate heat transfer correlation is used for estimating the wall-to-air heat transfer coefficient.

2.2. Governing equations

One-dimensional mass, momentum and energy conservation equations for the loop fluid, while flowing in vertically upward direction (assumed as the positive direction) through a tube of constant circular cross-section, can be presented as,

$$\frac{\partial \rho}{\partial t} + \frac{\partial G}{\partial z} = 0 \tag{1}$$

$$\frac{\partial G}{\partial t} + \frac{\partial}{\partial z}\left(\frac{G^2}{\rho}\right) = -\frac{\partial p}{\partial z} - \frac{f_{\text{in}}}{d_{\text{in}}}\left(\frac{G^2}{2\rho}\right) - \rho g \tag{2}$$

$$\rho C_p \frac{\partial T}{\partial t} + G C_p \frac{\partial T}{\partial z} = \frac{\partial}{\partial z}\left(\lambda \frac{\partial T}{\partial z}\right) - \left(\frac{4}{d_{\text{in}}}\right) H_{\text{in}}(T - T_w) \tag{3}$$

Here G is the mass flux of the loop fluid, d_{in} is the loop inner diameter and f_{in} is the wall friction factor. The fluid is always in contact with the wall material only, not the source, or the sink, and hence gains energy solely via convection with it, direction of heat transfer depending upon the sign of temperature difference. Here H_{in} describes the associated heat transfer coefficient.

The system under consideration operates in a loop driven by buoyancy and no other external factors, and hence the pressure drop around the loop has to be zero. Performing a cyclic integration of the fluid momentum equation (2) around the loop and applying Boussinesq approximation in the body force term to describe density as a linear function of local temperature, one obtains:

$$\oint -\Delta p = 0 \quad \Rightarrow \quad L_{\text{tot}} \frac{\mathrm{d}G}{\mathrm{d}t} + \left(\frac{f_{\text{in}} L_{\text{tot}}}{d_{\text{in}}}\right)\left(\frac{G^2}{2\rho}\right) + \rho_0 g \beta_{\text{av}} \oint (T_{\text{ref}} - T)\,\mathrm{d}z = 0 \tag{4}$$

Here L_{tot} is the total loop length, β_{av} is the volume expansion coefficient corresponding to the fluid temperature averaged over the total loop length (L_{tot}) and ρ_0 is the reference value of fluid density, corresponding to the reference temperature T_{ref}. Inlet temperature of the cooling stream at the cooler is chosen as the reference temperature.

The wall material is subjected to constant power input in the heater section (AB), convective heat transfer in the cooler section (CD) and also convective heat loss to the ambient in other uninsulated sections (BC and DA). It also exchanges heat with the loop fluid along the entire length of the loop (L_{tot}) through convection. Hence, there will be three different versions of the wall energy equation to recognize the multiple nature of energy exchange. The respective wall energy equation for the heater

section (AB), the cooler section (CD) and other uninsulated sections (BC and DA) can be represented as follows:

$$\rho_w C_{pw}\frac{\partial T_w}{\partial t} = \frac{\partial}{\partial z}\left(\lambda_w \frac{\partial T_w}{\partial z}\right) - H_{\text{in}} A_{\text{in}} \frac{(T_w - T)}{V_w} + \frac{\dot{Q}}{V_w} \quad (5a)$$

$$\rho_w C_{pw}\frac{\partial T_w}{\partial t} = \frac{\partial}{\partial z}\left(\lambda_w \frac{\partial T_w}{\partial z}\right) - H_{\text{in}} A_{\text{in}} \frac{(T_w - T)}{V_w} - H_{\text{ex}} A_{\text{out}} \frac{(T_w - T_{\text{ex}})}{V_w} \quad (5b)$$

$$\rho_w C_{pw}\frac{\partial T_w}{\partial t} = \frac{\partial}{\partial z}\left(\lambda_w \frac{\partial T_w}{\partial z}\right) - H_{\text{in}} A_{\text{in}} \frac{(T_w - T)}{V_w} - H_a A_{\text{out}} \frac{(T_w - T_a)}{V_w} \quad (5c)$$

Here $\dot{Q}$ is the power input from an external source, T_a is the ambient temperature and H_{ex} and H_a represent the heat transfer coefficients associated with wall-to-coolant and wall-to-air heat transfer, respectively. A_{in} and A_{out} are the inner and outer surface area of the wall segment under consideration, whereas V_w is the volume of corresponding wall material.

Temperature profile of the coolant stream can be obtained by simultaneously solving the associated energy equation. Expressed as:

$$\rho_{\text{ex}} C_{p\text{ex}}\frac{\partial T_{\text{ex}}}{\partial t} + G_{\text{ex}} C_{p\text{ex}}\frac{\partial T_{\text{ex}}}{\partial z} = \frac{\partial}{\partial z}\left(\lambda_{\text{ex}}\frac{\partial T_{\text{ex}}}{\partial z}\right) + H_{\text{ex}} A_{\text{out}} \frac{(T_w - T_{\text{ex}})}{V_{\text{ex}}} \quad (6)$$

Here G_{ex} is the coolant mass flux and V_{ex} is the coolant volume in that segment.

2.3. Heat transfer and friction factor correlations

It is observed that a suitable heat transfer correlation developed exclusively for natural circulation systems and applicable over wide range of parameters is not available in the literature. In view of this Petukhov correlation with Gnielinski modification [24] has been used for estimating the heat transfer coefficients for the fluid streams under turbulent condition ($Re > 2300$). This correlation is reported to have an error margin of $\pm 10\%$ over a wide range of Re values and hence, has successfully found extensive application in recently reported studies related to refrigeration and heat exchanger research, in particular. For a system with diameter d, associated Nu is given as

$$Nu_d = \frac{H_d L}{\lambda_f} = \frac{(f/8)(Re_d - 1000)Pr_f}{1 + 12.7(f/8)^{1/2}(Pr_f^{2/3} - 1)} \quad (7)$$

Friction factor relationship for turbulent flow has been taken in accordance with the corresponding heat transfer correlation as,

$$f = \left(0.79\ln(Re_d) - 1.64\right)^{-2} \quad (8)$$

Friction factor for laminar flow is given as $f = 64/Re_d$ and Nu in laminar flow for pipe diameter of d is defined based on associated Graetz number value [25] as,

$$Nu_d = \begin{cases} 1.86 Re_d^{1/3} Pr_f^{1/3} \left(\frac{d}{L_{\text{tot}}}\right)^{1/3} \left(\frac{\mu_f}{\mu_{\text{bulk}}}\right)^{0.14} & \text{for } Gz > 10 \quad (9a) \\ 3.66 & \text{for } Gz \leqslant 10 \quad (9b) \end{cases}$$

For estimation of wall-to-air heat transfer coefficient (H_a), the riser and downcomer tubes can be considered as vertical cylinders. Due to the absence of any widely-recognised correlation for natural convection for vertical cylinders, the correlation proposed by Churchill and Chu [26] for a vertical flat plate has been employed. Hence Nu_a for a length L is given as,

$$Nu_a = \frac{H_a L}{\lambda_a} = \left\{0.825 + \frac{0.387 Ra_L^{1/6}}{[1 + (0.492/Pr_a)^{9/16}]^{8/27}}\right\}^2 \quad (10)$$

2.4. Non-dimensionalisation of governing equations

Governing equations described in Section 2.2 can be non-dimensionalised using suitable reference parameters given by:

$$Z = \frac{z}{L_{\text{tot}}}, \qquad \widehat{G} = \frac{G}{G_{\text{ss}}}$$
$$\tau = \frac{t}{(L_{\text{tot}}/U_{\text{ss}})}, \qquad \theta = \frac{T - T_{\text{ref}}}{\Delta T_{\text{ref}}}$$
$$\hat{\rho} = \frac{\rho}{\rho_0}, \qquad \widehat{C}_p = \frac{C_p}{C_{p0}}, \qquad \hat{\mu} = \frac{\mu}{\mu_0}, \qquad \hat{\lambda} = \frac{\lambda}{\lambda_0} \quad (11)$$

Here all the reference property values correspond to working fluid property at reference temperature (T_{ref}). Steady state velocity is defined as, $U_{\text{ss}} = G_{\text{ss}}/\rho_0$, whereas the temperature variables have been non-dimensionalised using a reference temperature drop, defined as $\Delta T_{\text{ref}} = \dot{Q}/G_{\text{ss}} A_{\text{cs}} C_{p0}$.

Use of non-dimensional parameters converts the loop momentum equation (4) and energy equation (4) into the following form.

$$\hat{\rho}\widehat{C}_p\frac{\partial\theta}{\partial\tau} + \widehat{G}\widehat{C}_p\frac{\partial\theta}{\partial Z} = \left(\frac{d_{\text{in}}}{L_{\text{tot}}}\right)\frac{1}{Re_{\text{ss}}Pr_0}\frac{\partial}{\partial Z}\left(\hat{\lambda}\frac{\partial\theta}{\partial Z}\right) - (St_m)_{\text{in}}(\theta - \theta_w) \quad (12)$$

$$\frac{\mathrm{d}\widehat{G}}{\mathrm{d}\tau} + \left(\frac{f_{\text{in}} L_{\text{tot}}}{2d_{\text{in}}}\right)\left(\frac{\widehat{G}^2}{\hat{\rho}}\right) - \left(\frac{L_{\text{tot}}}{h}\right)\frac{Gr_m}{Re_{\text{ss}}^3}\oint \theta \hat{g}_z \,\mathrm{d}Z = 0 \quad (13)$$

Here $\hat{g}_z$ represents the direction of gravity force along loop length. For the riser tube, its value is $+1$, along downcomer it is -1 and 0 in horizontal arms.

Three different versions of wall energy equation (5) convert to the following forms:

$$\hat{\rho}_w\widehat{C}_{pw}\frac{\partial\theta_w}{\partial\tau} = \left(\frac{d_{\text{in}}}{L_{\text{tot}}}\right)\frac{1}{Re_{\text{ss}}Pr_0}\frac{\partial}{\partial Z}\left(\hat{\lambda}_w\frac{\partial\theta_w}{\partial Z}\right) - (St_m)_{\text{in}} R_{\text{in}}(\theta_w - \theta) + \frac{\dot{Q} R_{\text{in}}}{G_{\text{ss}} A_{\text{cs}} C_{p0}\Delta T_{\text{ref}}}\left(\frac{L_{\text{tot}}}{L_h}\right) \quad (14a)$$

$$\hat{\rho}_w\widehat{C}_{pw}\frac{\partial\theta_w}{\partial\tau} = \left(\frac{d_{\text{in}}}{L_{\text{tot}}}\right)\frac{1}{Re_{\text{ss}}Pr_0}\frac{\partial}{\partial Z}\left(\hat{\lambda}_w\frac{\partial\theta_w}{\partial Z}\right) - (St_m)_{\text{in}} R_{\text{in}}(\theta_w - \theta) - (St_m)_{\text{ex}} R_{\text{out}}(\theta_w - \theta_{\text{ex}}) \quad (14b)$$

$$\hat{\rho}_w\widehat{C}_{pw}\frac{\partial\theta_w}{\partial\tau} = \left(\frac{d_{\text{in}}}{L_{\text{tot}}}\right)\frac{1}{Re_{\text{ss}}Pr_0}\frac{\partial}{\partial Z}\left(\hat{\lambda}_w\frac{\partial\theta_w}{\partial Z}\right) - (St_m)_{\text{in}} R_{\text{in}}(\theta_w - \theta) - (St_m)_a R_{\text{out}}(\theta_w - \theta_a) \quad (14c)$$

External fluid energy equation (6) can similarly be represented as,

$$\hat{\rho}_{\mathrm{ex}}\widehat{C}_{p\mathrm{ex}}\frac{\partial\theta_{\mathrm{ex}}}{\partial\tau}+\widehat{G}_{\mathrm{ex}}\widehat{C}_{p\mathrm{ex}}\frac{\partial\theta_{\mathrm{ex}}}{\partial Z}=\left(\frac{d_{\mathrm{in}}}{L_{\mathrm{tot}}}\right)\frac{1}{Re_{\mathrm{ss}}Pr_0}\frac{\partial}{\partial Z}\left(\hat{\lambda}_{\mathrm{ex}}\frac{\partial\theta_{\mathrm{ex}}}{\partial Z}\right)+(St_m)_{\mathrm{ex}}R_{\mathrm{ex}}(\theta_w-\theta_{\mathrm{ex}}) \tag{15}$$

A number of dimensionless parameters have been used in the equations mentioned above.

$$Re_{\mathrm{ss}}=\frac{G_{\mathrm{ss}}d_{\mathrm{in}}}{\mu_0},\qquad Pr_0=\frac{\mu_0C_{p0}}{\lambda_0},\qquad Gr_m=\frac{g\beta_{\mathrm{av}}d_{\mathrm{in}}^3\rho_0^2\dot{Q}h}{A_{\mathrm{cs}}\mu_0^3C_{p0}}$$

$$(St_m)_{\mathrm{in}}=\frac{(4L_{\mathrm{tot}}/d_{\mathrm{in}})Nu}{Re_dPr},\qquad (St_m)_{\mathrm{ex}}=\frac{(4L_{\mathrm{tot}}/d_{\mathrm{in}})Nu_{\mathrm{ex}}}{Re_{d\mathrm{ex}}Pr_{\mathrm{ex}}}$$

$$(St_m)_a=\frac{(4L_{\mathrm{tot}}/d_{\mathrm{in}})H_a}{\rho_0C_{p0}U_{\mathrm{ss}}},\qquad R_{\mathrm{in}}=\frac{d_{\mathrm{in}}^2}{d_{\mathrm{out}}^2-d_{\mathrm{in}}^2}$$

$$R_{\mathrm{out}}=\frac{d_{\mathrm{out}}^2}{d_{\mathrm{out}}^2-d_{\mathrm{in}}^2},\qquad R_{\mathrm{ex}}=\frac{d_{\mathrm{out}}^2}{d_{\mathrm{ex}}^2-d_{\mathrm{out}}^2} \tag{16}$$

As has already been mentioned earlier, the operation of NCL depends on the interplay between frictional and gravitation forces. Among the dimensionless groups introduced in Eq. (16), modified Grashof number (Gr_m) serves as an indication of driving buoyancy force, whereas Reynolds number (Re) is representative of flow inertia, which in turn, is proportional to loop friction. Hence, these two parameters are expected to suitably depict the phenomenon and hence characterize the system performance. Both being direct functions of important geometric parameters such as loop diameter and height, variation in system geometry will always get reflected in their values and hence, corresponding system response can satisfactorily be represented by them. Modified Stanton number illustrates the heat transfer behaviour between the wall and the fluids and can be used to explain the temperature profiles and hence the values of average volumetric expansion coefficient of the fluid, which, in turn, has a significant effect on Gr_m and thus on driving head as well. Hence these dimensionless groups are capable of portraying the complete system behaviour, along with the temperature profiles and heat leakage.

2.5. Solution procedure

Eqs. (12)–(15) describe the complete steady state and dynamic behaviour of the entire system under consideration (Fig. 1). Temperature profile of the loop fluid, wall material and coolant stream, and the loop flow rate can be estimated through simultaneous solution of this set of coupled equations. As the system under consideration is a NCL, there is no explicit boundary condition. The power input to the system ($\dot{Q}$) and the flow rate and inlet temperature of the cooling stream provides the external controlling parameters. In order to obtain the desired static solutions, a pseudo-steady approach has been followed with finite volume discretization technique. Optimum number of grid points and convergence criteria has been determined through a trade-off between desired level of accuracy and solution time requirement. Because of the transient nature of the solution procedure, initial condition is needed to be specified. In order to avoid unnecessary oscillations, which may arise during buoyancy-induced flow build-up from absolute zero velocity level, natural circulation is assumed to be initiated by a forced flow, for example, by tripping a pump and switching on the heater and cooling stream simultaneously. Time-marching solution has been allowed till an accuracy level of 10^{-5}.

Properties of the working fluid, i.e., water has been estimated from an indigenously developed property code, following the guidelines adopted by International Association for the Properties of Water and Steam (IAPWS-IF 97) [27]. Properties of wall material (AISI 302 stainless steel) and air have been taken from standardized property tables [28]. For a completely enclosed system, due to the greater thermal expansion of liquid compared to the solid wall, system pressure is expected to be higher than atmospheric and hence an assumed constant system pressure value of 3 bar has been maintained throughout the present study. Cooling water inlet temperature is specified as 20 °C, which closely matches the available water source in the laboratory where a test loop is being erected. A coolant mass flow rate value of 0.163 kg s^{-1} has been chosen, which yields an approximate inlet velocity of 10 cm s^{-1} through a 10 mm annular passage around the top horizontal arm (CD in Fig. 1), for a system with 40 mm internal diameter. Cooling stream conditions are expected to have significant effect on system performance, which is beyond the scope of the present study.

3. Results and discussion

Steady-state solution of the coupled equations (12)–(15) generates the temperature profile for loop fluid, wall material and coolant stream. Basic nature of the profiles has already been reported by Basu et al. [23]. Increase in wall and fluid temperature across the heater is very much identical, and so is the decrease across the cooler section. However, at any location along the loop, there is a gap of a few degrees between the wall and the fluid, implying a high thermal resistance between them. It is not possible to have highly turbulent flow in buoyancy-driven systems like NCL, and so the heat transfer coefficient (H_{in}) is lower compared to forced flow situations. Sudden change in wall temperature has been observed on either end of heat-exchanging sections, indicating the dominant nature of convection over wall conduction. Wall temperature changes considerably along the bare sections, showing the influence of heat loss to ambient and also justifying the utility of considering wall heat loss in the study of NCL.

3.1. Model validation

Predictions from the present numerical model have been compared with experimental data presented by Mousavian et al. [29], which considered a circuit of two horizontal copper tubes (heat exchanging sections) and two vertical stainless steel tubes (assumed adiabatic), connected by four 90° stainless steel

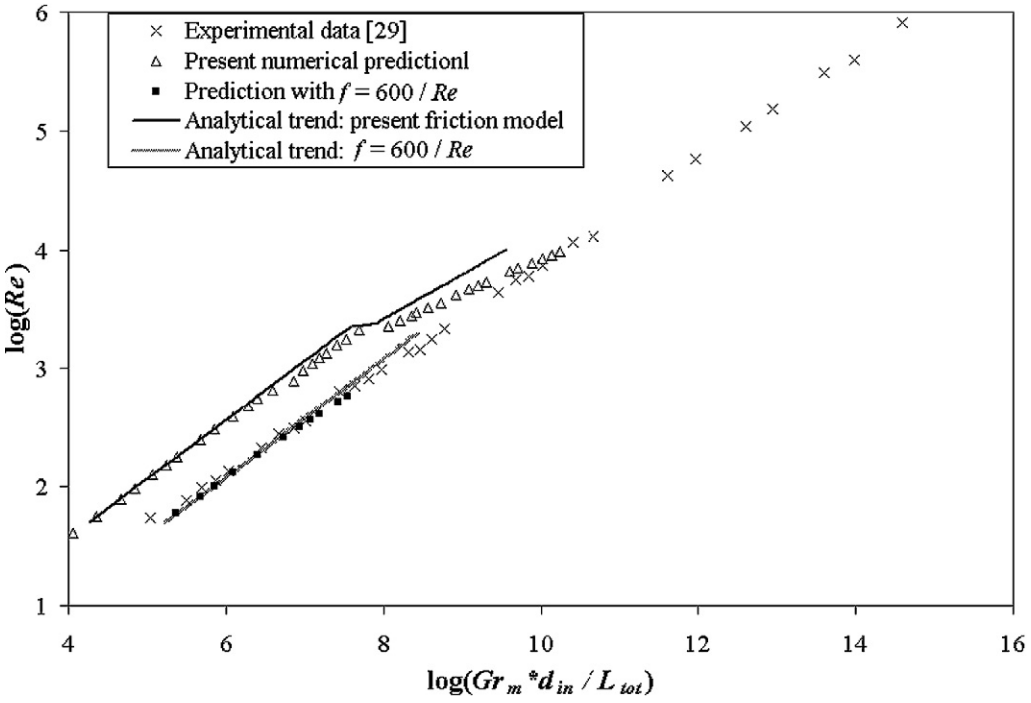

Fig. 2. Comparison of numerical prediction with corresponding experimental results [29].

bends. A similar configuration has been analysed where adiabatic condition has been implied setting H_a equal to zero. The input power is varied from a few Watt to kilo Watt range yielding a wide range of Re (from about 50 to about 10^4). Corresponding values of Gr_m range from 10^6 to 10^{12}. As can be seen from Fig. 2, predicted results are in close agreement with the experimental data in the turbulent regime ($Re > 2300$), and nearly match the reported values at higher flow rates (for $Re > 4000$). Observed small difference can be attributed to the employed correlations. The Petukhov correlation [24] and the corresponding friction factor estimate reportedly have an error margin of $\pm 10\%$ [28]. Use of Blasius relationship and Churchill relationship [28], with relative roughness value of 0.001, results in nearly an identical prediction.

However, a larger discrepancy occurs in the laminar regime. Predicted values follow an identical slope, but with much higher estimation of Re for a given Gr_m value, indicating a lesser friction. Vijayan et al. [18] has predicted the presence of higher frictional losses in natural circulation systems compared to forced flow ones, for identical Re. In fact, use of an arbitrary friction factor relation of $f = 600/Re_d$ provides a nearly accurate prediction. Such trends clearly emphasize the fact that the knowledge from channel forced flow study cannot be applied indiscriminately to natural circulation systems. It is a topic of fundamental research and more detailed investigations are needed before reaching any conclusion regarding the nature of flow regimes in NCL systems and applicable heat transfer relations.

To have a better understanding, the predicted results have also been compared with approximate analytical prediction following the approach of Vijayan [21]. Neglecting the effect of wall heat conduction and heat loss to ambient, Eq. (13) gives rise to a closed-form relation between Re and Gr_m under steady-state condition. The resulting profile has been plotted in Fig. 2 to facilitate comparison, using both the present friction factor model and the arbitrary relation of $f = 600/Re_d$. A change can be observed in the slope of the profile for the present friction model, which may be attributed to the use of different correlations for laminar and turbulent regime. The results exhibit fairly good agreement with the numerical prediction, but they diverge slightly for higher Re values, which may be indicative of enhanced role of wall conduction due to higher heat transfer coefficients. The comparison presented here is for a narrow range; it was not possible to achieve even higher Re values due to saturation temperature limit of water at the given pressure and as no clear mention is made in the reported work [29] about associated pressure condition. However, the cases considered in the following sections are well inside the turbulent region and hence, can be considered to be close to practical situation.

3.2. Effect of loop height (h)

The driving force in a NCL is the density difference of working fluid flowing upwards in the riser and downwards in the downcomer. Hence the vertical arms play a critical role in generating the required buoyancy force. Fig. 3 shows the effect of loop height on steady state Re and Gr_m for both ideally insulated system ($H_a = 0$) and uninsulated system open to ambient at 20 °C temperature. Both Re and Gr_m are found to increase with h, but with different gradients. According to the present definition of Gr_m (Eq. (16)), for a loop with constant cross-sectional area and constant power supply, $Gr_m = Gr_m(h, \beta_{av})$. Gr_m is linearly proportional to both these parameters and loop behaviour will depend upon their relative influence.

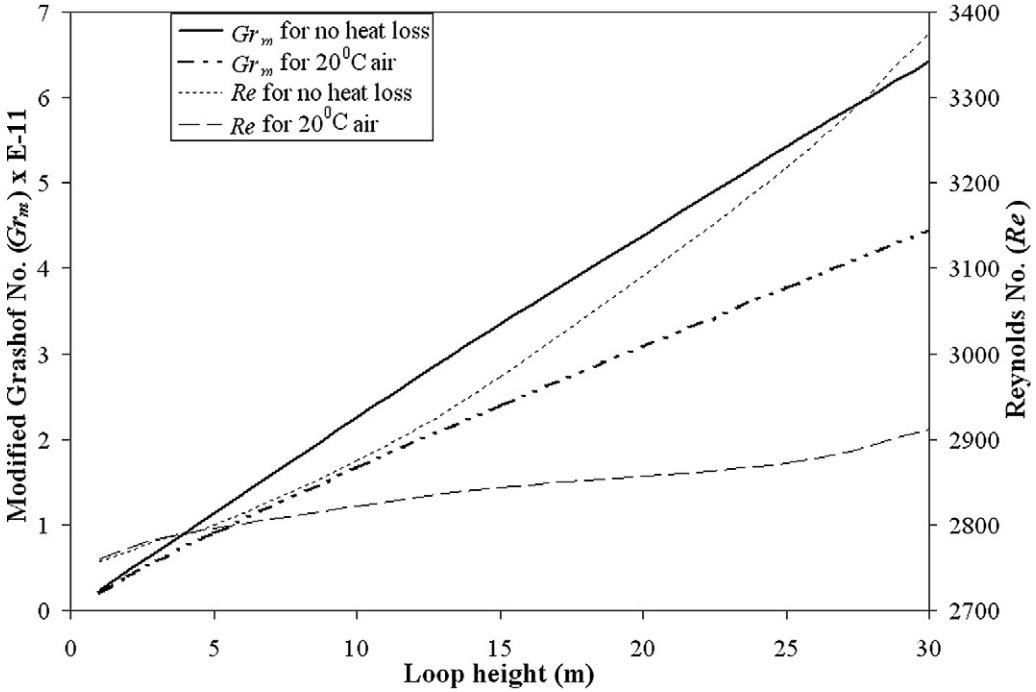

Fig. 3. Effect of loop height on modified Grashof number (Gr_m) and Reynolds number (Re), where $L_h = 1.4$ m, $L_c = 1.2$ m, $d_{in} = 40$ mm and $\dot{Q} = 500$ W.

Table 1
Effect of loop height on averaged values of wall and fluid temperature and modified Stanton number

Loop height (m)	No heat loss to air			Heat loss to air at 20 °C		
	$[T_w]_{av}$ (K)	$[T]_{av}$ (K)	$[(St_m)_{in}]_{av}$	$[T_w]_{av}$ (K)	$[T]_{av}$ (K)	$[(St_m)_{in}]_{av}$
1	313.29	313.20	0.775	308.92	308.91	0.725
2	313.23	313.13	1.087	307.34	307.04	0.986
3	313.13	313.04	1.398	305.89	305.38	1.234
5	313.02	312.92	2.020	304.05	303.25	1.717
10	312.51	312.41	3.560	301.73	300.55	2.889
15	311.91	311.82	5.081	300.52	299.13	4.032
25	310.58	310.50	8.034	299.23	297.62	6.284
30	309.84	309.76	9.480	298.79	297.14	7.414

Despite change in loop height, wall material is receiving the same amount of power over the same length in heater section (AB in Fig. 1). Also there is no heat loss to ambient under ideally insulated condition. So the wall material follows nearly identical profile, with small decrease in average temperature (averaged over the entire loop length), as can be seen from Table 1. Therefore fluid temperature follows the same pattern, resulting in small decrease in β_{av}. A change of loop height (h) from 1 to 30 m causes a decrease in average fluid temperature by about 3.5 K (Table 1). That corresponds to a decrease in β_{av} by only about 6.9%. So Gr_m is practically a near-linear function of h and increases monotonically with increase in loop height.

As loop mass flow rate is decided by interplay between friction and buoyancy forces [4], increase in Gr_m indicates a proportional increase in buoyancy. So the friction force must increase to maintain the self-correcting balance of NCL. That results in an increase in loop mass flow rate and also in Re, as shown in Fig. 3. Also, as the fluid density increases at lower temperature and friction force can be shown to be inversely dependent on fluid density, higher density acts as additional incentive to increase Re at higher values of h. Wall-to-fluid heat transfer coefficient (H_{in}) is a complex function of Re and Pr. For the same Re value, lower fluid temperature is found to produce slightly lower value of H_{in}. So increase in loop height produces a rapid increase in $(St_m)_{in}$ (Table 1), resulting in enhanced heat transfer from wall to loop fluid and leading to a drop in average wall temperature, as mentioned above. Local wall temperature is the highest at the outlet to heater (point B in Fig. 1) and that can be taken as an indication of the direction of change in overall wall behaviour. Fig. 4 shows the continuous drop in wall temperature at heater outlet with increase in loop height (h) for an ideally insulated system.

However, when the system is exposed to the ambient, heat transfer occurs between hot wall and the cooler surrounding, thereby considerably reducing the wall temperature. Increase in loop height provides greater surface area for heat exchange between wall and ambient leading to increased heat loss. As can be seen from both Fig. 4 and Table 1, for any particular loop height, wall temperature at heater outlet and average wall temperature for 20 °C ambient is considerably lower than those for ideally insulated condition and the gap opens up with increasing loop height, suggesting higher heat loss to ambient. Lower wall temperature simultaneously reduces the fluid temperature as well. A change in h from 1 to 30 m causes average fluid temperature to drop by more than 10 K, resulting in almost 30% decrease in β_{av}. Reduced volume expansion counteracts the increase in height and hence Gr_m increases with a much flatter profile (Fig. 3). A similar trend is observed for Re as well. So local heat transfer coefficient increases with height, but at a reduced rate. However, increase in fluid density seems to increase Re slightly for a very high value of h.

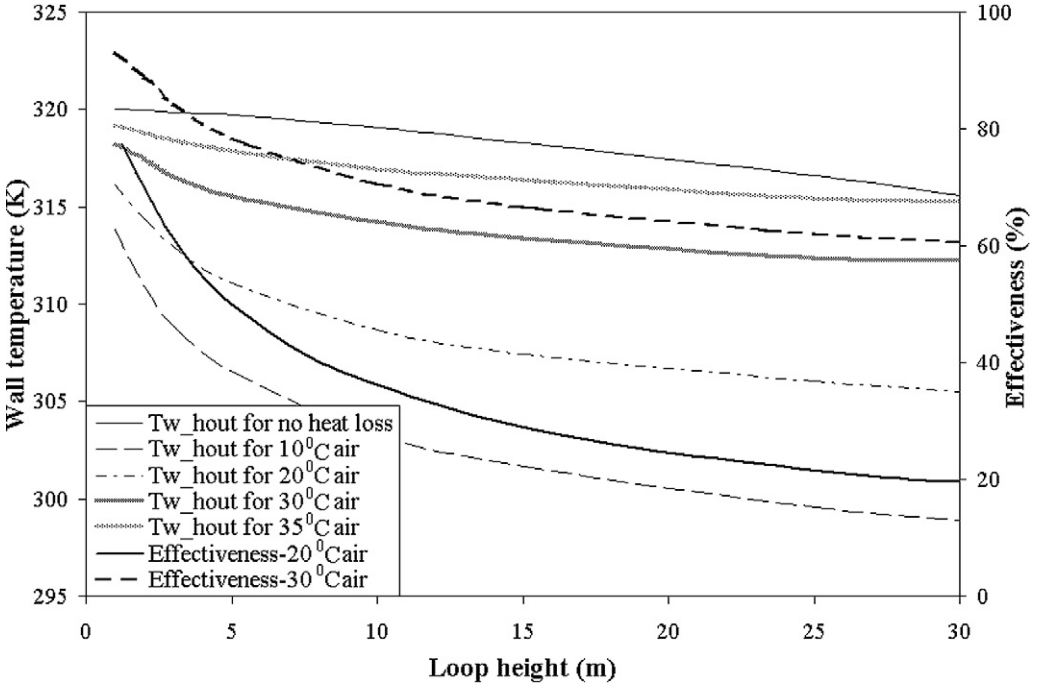

Fig. 4. Effect of loop height on wall temperature at heater outlet and system effectiveness (ε) for different ambient conditions.

General application areas of single-phase NCLs mostly concentrate on efficient transfer of energy from a high-temperature source to a low-temperature sink, as in case of the primary circulation loop of a liquid metal-cooled fast breeder reactor. Loss of heat from wall to ambient is bound to affect the very purpose of the system. Increase in coolant temperature across the cooler indicates the amount of energy going to the cooling stream. As can be seen from Fig. 5, with increase in loop height in an ambient of 20 °, there is a sharp decrease in coolant outlet temperature. The difference is more pronounced at smaller loop heights, because of the higher percentage increase in outer surface area at smaller heights compared to their higher counterparts. Defining system effectiveness as the fraction of input power going to the cooling stream ($\varepsilon = \dot{m}_{\mathrm{ex}} \int_{L_c} C_{p\mathrm{ex}}\, \mathrm{d}T_{\mathrm{ex}}/\dot{Q}$), i.e., the usable fraction of $\dot{Q}$, it is observed that with increase in h, there is a sharp decrease in effectiveness, particularly at lower heights (Fig. 4). However, increased ambient temperature reduces the wall-to-air thermal gradient leading to reduced heat loss, as reported earlier by Basu et al. [23]. Thus wall temperature level increases yielding higher system effectiveness (Fig. 4). Profile of wall temperature at heater outlet for 35 ° ambient is much closer to the no-heat-loss profile, compared to that for 10 or 20 ° ambient conditions.

As increase in loop height reduces system effectiveness and cooler ambient results in increased heat loss from loop wall, taller loops are expected to give much poorer performance under low ambient temperature conditions. As is shown in Fig. 6, for 10 ° ambient, effectiveness drops drastically with increase in loop height (h). In fact, for loops taller than 10 m, it is possible to attain the trivial situation of negative effectiveness. For such cases, due to the large exposed surface to a very cold surrounding, extensive heat loss takes place, causing the wall temperature at cooler inlet to become even less than the coolant inlet temperature and so heat transfer occurs from external fluid to wall. Hence lower coolant outlet temperature yields negative effectiveness and thereby completely altering the basic purpose of the system. So it is advantageous to have smaller loop height and preferably higher ambient temperature in order to have better output from the system. However, if the objective is to have larger mass flow rate, taller loops are a better option.

3.3. Effect of loop width (W)

A wider loop having the same heater length provides greater flow path. Under no-heat-loss condition, wall temperature and hence fluid temperature exhibits nearly identical profiles. β_{av} remains about the same and a fixed value of h leads to a near-constant value of Gr_m over a wide range of W (Fig. 7).

However, when heat loss to ambient is considered, along with appropriate correlation to estimate wall-to-air heat transfer coefficient for the horizontal sections [30], longer horizontal arms provide additional surface for heat transfer. That brings the wall temperature down along with the average fluid temperature. Associated lowering of β_{av} results in a steady drop in Gr_m with increase in W (Fig. 7). Increase in W from 1.4 m to 6.4 m causes a decrease in β_{av} by about 16%. Such heat loss results in significant deterioration in system effectiveness (ε), as shown in Fig. 7.

3.4. Effect of heater length (L_h)

Reduction in heater length, keeping all other geometric parameters the same, increases loop Reynolds number (Re). However, for a change in heater length from 1.4 m to 0.8 m under ideally insulated condition, the change in Re is quite moderate (Fig. 8). Loop diameter and reference property values being the

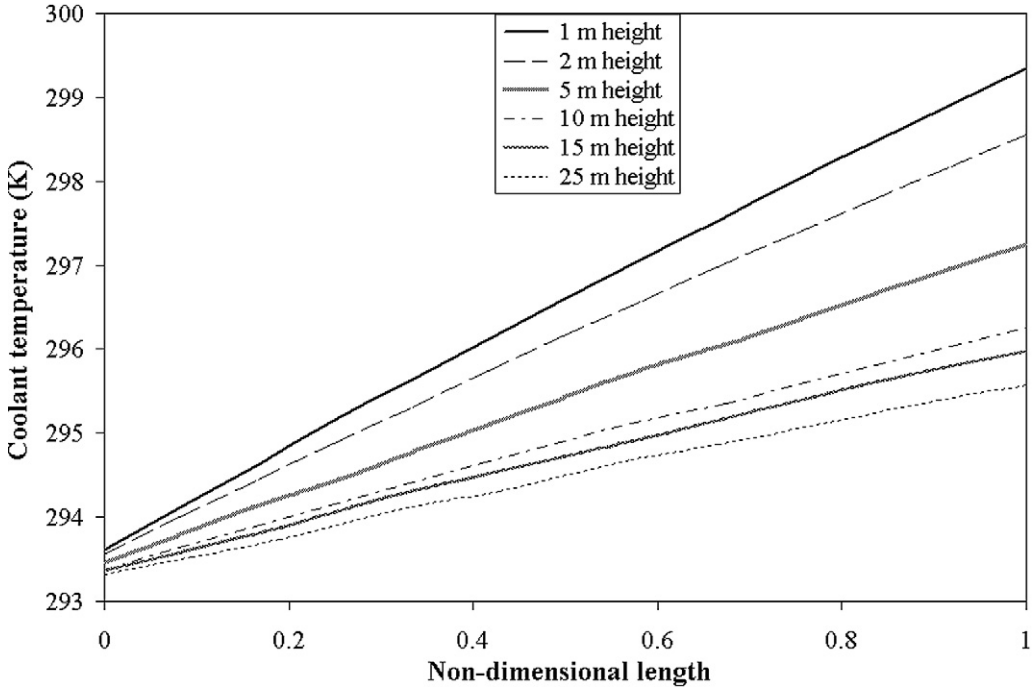

Fig. 5. Effect of loop height on coolant stream temperature profile for 20 ° ambient and 5 kW power supply.

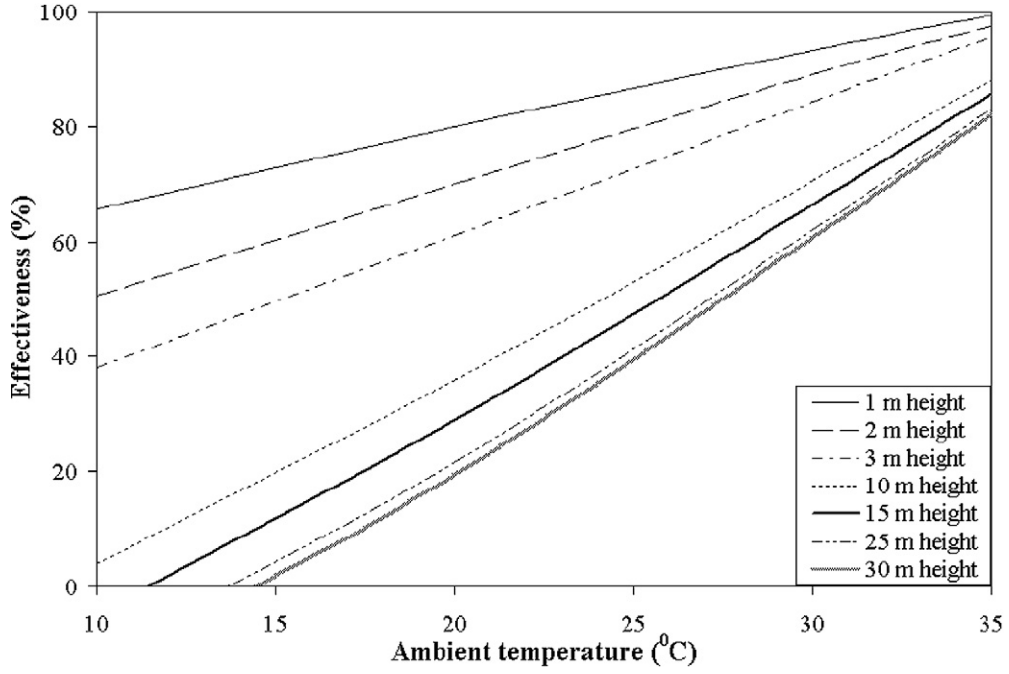

Fig. 6. Combined effect of loop height and ambient temperature on system effectiveness (ε) for 500 W heat input.

same, increase in *Re* implies a corresponding increase in loop flow rate and hence, for constant power input to the system, decrease in average loop fluid temperature (Table 2). Heat transfer coefficient being a direct function of *Re* and *Pr*, and change in *Pr* corresponding to average fluid temperature being negligibly small, such small changes in *R*e results in nearly the same value of H_{in}. Now reduction in heater length with constant power input increases the wall heat flux ($=\dot{Q}/\pi d_{\text{in}} L_h$). Thermal resistance per unit surface area remaining the same with higher heat flux, electrical analogy suggests a higher temperature differential between the wall and the fluid. So wall temperature at heater outlet increases and fluid temperature decreases, leading to an overall increase in average wall temperature (Table 2). As can be seen from Fig. 9, for a decrease in heater length from 1.4 to 0.8 m under ideally insulated condition, there is a rise in T_w at heater outlet by about 4 K. Associated decrease in fluid temperature also reduces the value of β_{av}. As is already mentioned in Section 3.2, $Gr_m = Gr_m(h, \beta_{\text{av}})$; h being a con-

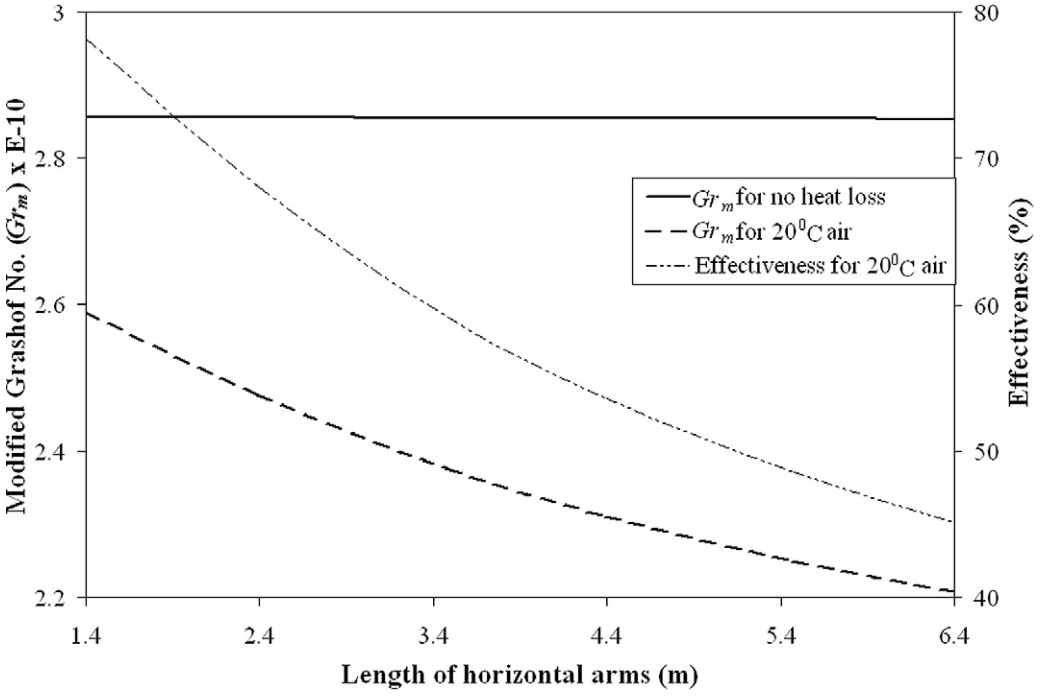

Fig. 7. Effect of uninsulated horizontal length on modified Grashof number (Gr_m) and system effectiveness (ε), where $L_h = 1.4$ m, $L_c = 1.2$ m, $h = 1.245$ m, $d_{\text{in}} = 40$ mm and $\dot{Q} = 500$ W.

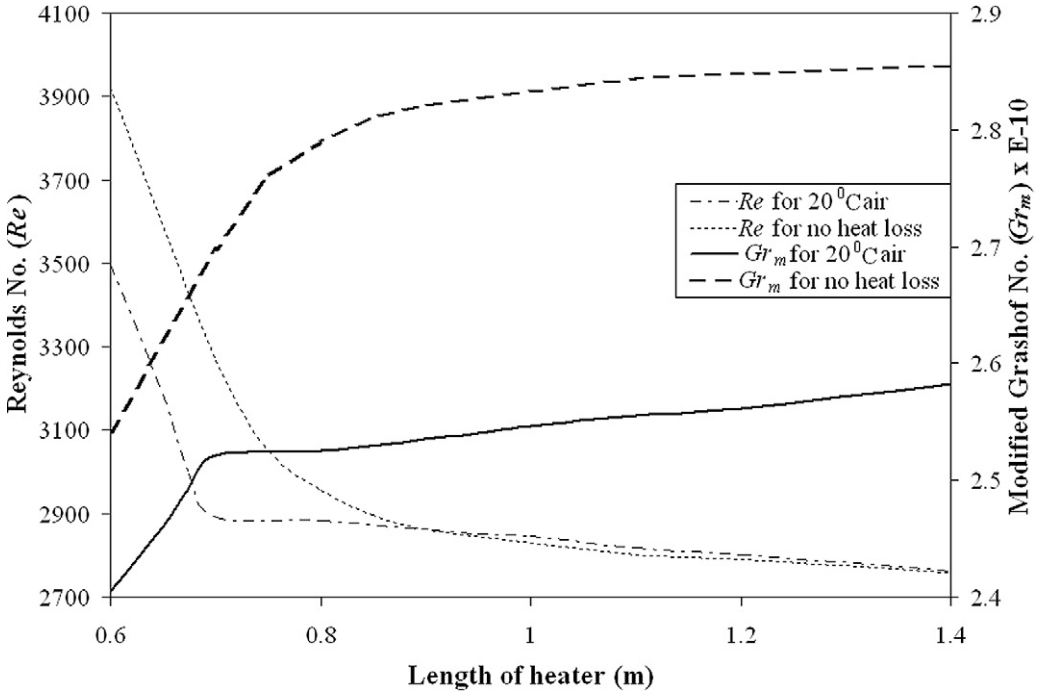

Fig. 8. Effect of heater length on modified Grashof number (Gr_m) and Reynolds number (Re), where $W = 1.48$ m, $h = 1.245$ m, $L_c = 1.2$ m, $d_{\text{in}} = 40$ mm and $\dot{Q} = 500$ W.

stant, $Gr_m = Gr_m(\beta_{\text{av}})$ in the present case. Table 2 shows that a reduction of heater length from 1.4 to 0.6 m for an ideally insulated system causes a decrease in β_{av} by about 11.5%, and hence implies an identical change in Gr_m.

As the heater length continues to be shorter, considerable amount of increase in the value of Re enhances the wall-to-fluid heat transfer. When the heater length goes below some particular value (about 0.8 m for no-heat-loss case), enhancement of heat transfer coefficient becomes sufficient to reduce the average temperature differential between wall and fluid. Average fluid temperature decreases sharply due to the increased thermal mass and higher specific heat of water. But the average value of wall temperature (Table 2) and wall temperature at heater outlet (Fig. 10) starts to decrease beyond that particular point. That

Table 2
Effect of heater length on averaged values of wall and fluid temperature and corresponding change in volume expansion coefficient

Length of heater (m)	No heat loss to air				Heat loss to air at 20 °C			
	$[T_w]_{av}$ (K)	$[T]_{av}$ (K)	% change in β_{av}	% change in Gr_m	$[T_w]_{av}$ (K)	$[T]_{av}$ (K)	% change in β_{av}	% change in Gr_m
1.4	313.28	313.19	0.0	0.0	308.54	308.44	0.0	0.0
1.2	313.32	312.99	−0.585	−0.245	308.58	308.11	−0.790	−0.800
1.0	313.37	312.63	−1.305	−0.771	308.65	307.79	−1.541	−1.390
0.9	313.48	312.49	−1.596	−1.191	308.77	307.63	−2.567	−1.727
0.8	313.20	311.92	−2.725	−2.277	308.94	307.46	−2.337	−2.223
0.7	311.81	310.28	−6.077	−5.499	309.27	307.35	−2.581	−2.352
0.6	309.40	307.66	−11.560	−10.998	307.64	305.54	−6.942	−6.879

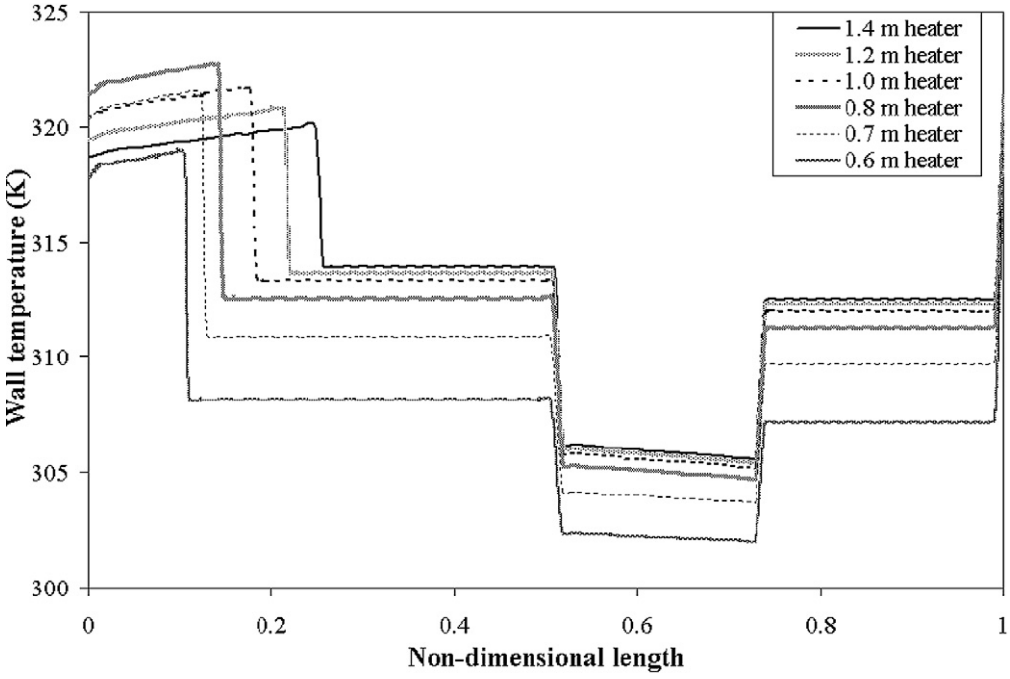

Fig. 9. Effect of heater length on wall temperature profile for ideally insulated condition.

also explains the reason behind reversal in positioning of the wall temperature profiles for very small heater lengths (Fig. 9). Lower average fluid temperature causes a rapid decrease in the value of β_{av} (Table 2), which results in significant variation in the profile of Gr_m, as can be seen from Fig. 8.

In earlier discussions, it was observed that the profiles of Gr_m and Re follow identical directions. However, when there is no change in the system diameter and height, $Gr_m = Gr_m(\beta_{av})$. Now β_{av} is a function of average loop fluid temperature, which in turn depends on loop flow rate and hence on Re. Higher value of Re implies a higher mass flow rate leading to lower temperature level of fluid, lower value of β_{av} and thus smaller Gr_m. So, for systems where Gr_m solely depends on β_{av}, profile of Gr_m and Re exhibits opposite trends, as is evident from the profiles in Fig. 8.

In presence of ambient heat loss, the same trends are replicated. However, lower fluid temperatures leads to a slower decrease in β_{av}, yielding a smaller gradient of Gr_m. Change of heater length from 0.7 to 0.6 m causes a sudden change in β_{av}, providing a sharp gradient in Gr_m profile beyond that point (Fig. 8). Re profile follows the same trend and so does the profile of T_w at heater outlet (Fig. 10). A smaller heater length provides greater surface exposed to the ambient and higher wall temperature provides a greater temperature differential, resulting in a reduction in system effectiveness (ε) with reduced heater length (Fig. 10). However, as wall temperature starts decreasing, effectiveness improves.

3.5. Effect of inner diameter (d_{in})

Internal diameter of the loop is an important parameter with respect to practical issues such as space requirement and manufacturing costs. Keeping wall thickness and annular passage of coolant stream the same, if d_{in} is increased, $Gr_m = Gr_m(d_{in}, \beta_{av})$, for the same loop height. A smaller diameter loop carries lower mass flow rate for the same power input and so temperature level is higher. With increase in diameter, average fluid temperature decreases, causing a reduction in β_{av}. Hence, Gr_m increases with loop diameter (Fig. 11), but with a gradient less than unity due to decrease in β_{av}. Increased buoyancy causes the flow rate and hence Re to increase with

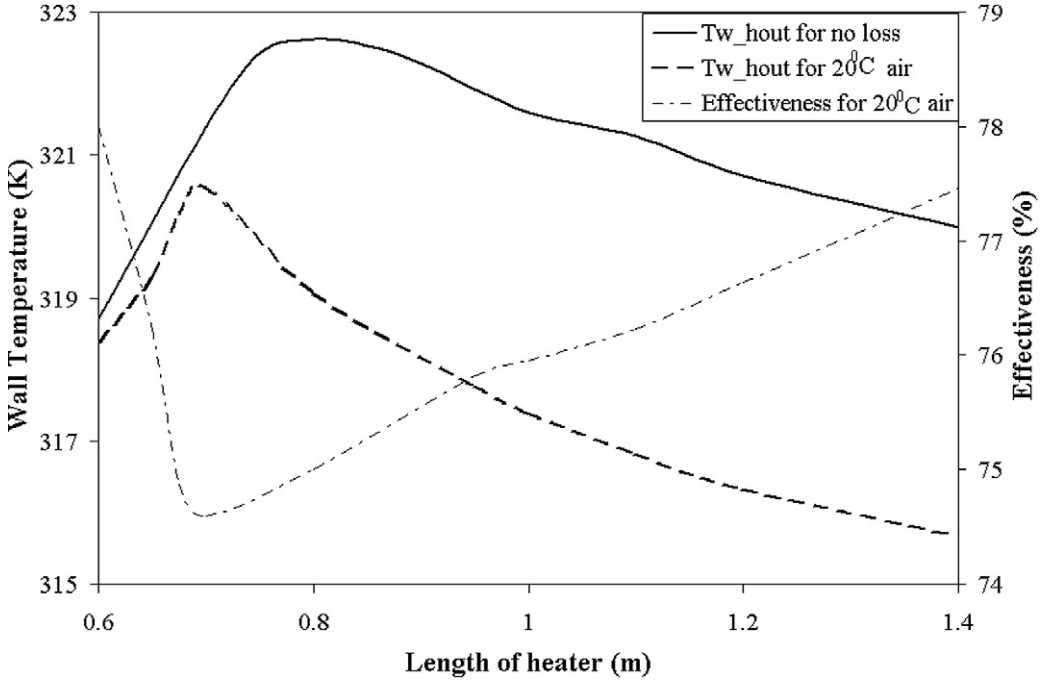

Fig. 10. Effect of heater length on wall temperature at heater outlet and system effectiveness (ε) for 20 °C ambient.

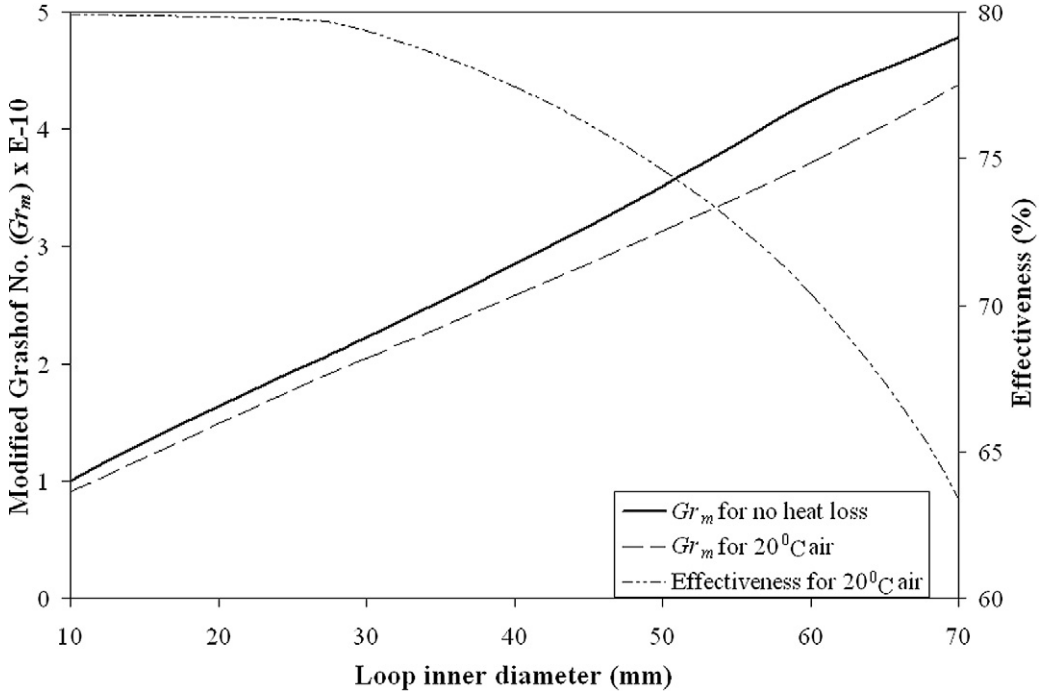

Fig. 11. Effect of loop inner diameter (d_{in}) on modified Grashof number (Gr_m) and system effectiveness (ε), where $L_h = 1.4$ m, $L_c = 1.2$ m, $h = 1.245$ m and $\dot{Q} = 500$ W.

diameter. When heat loss is under consideration, fluid temperature level is lower for the same system compared to no-heat-loss condition. Increased loop diameter allows increased surface area to be exposed to ambient leading to additional decrease in wall and fluid temperature. So Gr_m is lower and corresponding profile veers further away from the profile for perfectly insulated condition at larger diameters. That results in overall reduction in loop efficiency (ε), particularly for large diameters (Fig. 11), as was suggested by Basu et al. [23].

3.6. Effect of wall thickness ($(d_{out} - d_{in})/2$)

Increase in wall thickness increases the thermal mass of the wall material. That, in turn, increases the wall heat conduction effects and greater energy is required to cause any particular increase in T_w. Hence, for the same amount of power input to the system ($\dot{Q}$), with increase in wall thickness, wall temperature decreases and so does the fluid temperature. If height (h) and internal diameter (d_{in}) of the loop remains the same,

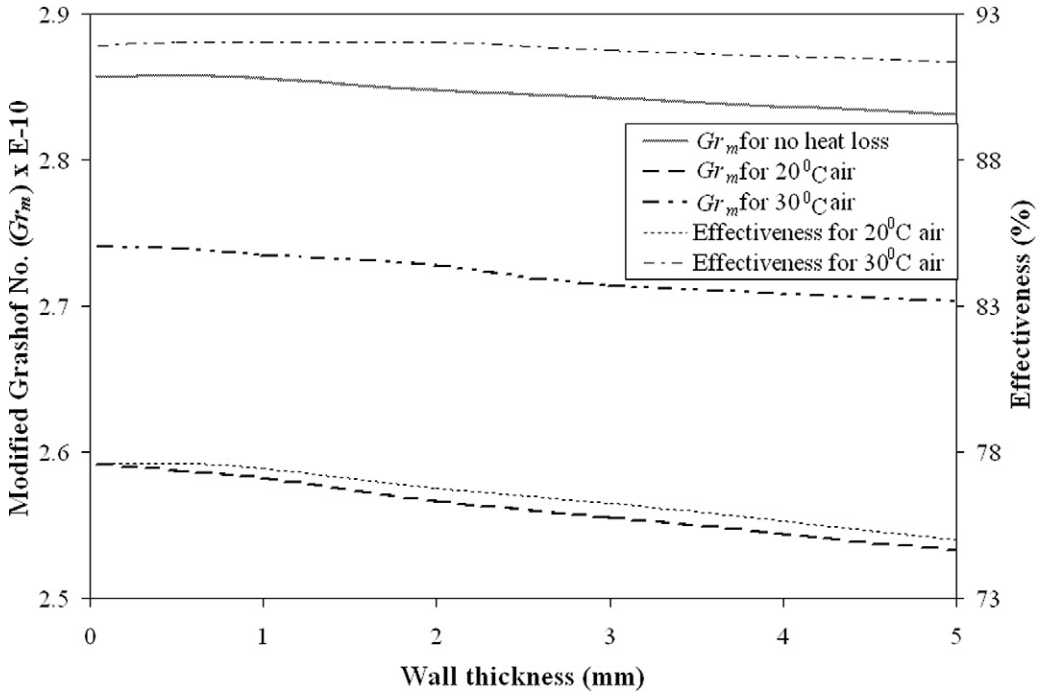

Fig. 12. Effect of wall thickness on modified Grashof number (Gr_m) and system effectiveness (ε), where $L_h = 1.4$ m, $L_c = 1.2$ m, $h = 1.245$ m, $d_{\text{in}} = 40$ mm and $\dot{Q} = 500$ W.

$Gr_m = Gr_m(\beta_{\text{av}})$. Lower fluid temperature yields lower β_{av} causing reduction in Gr_m. Fig. 12 exhibits a monotonic drop in Gr_m for thicker tubes. However, convection still remains the dominant mode of heat transport and hence the modest level of decrease in Gr_m (Fig. 12) and low averaged wall and fluid temperatures. When heat loss is under consideration, increase in wall thickness increases the outer diameter, thereby increasing the external surface area exposed to the ambient. Therefore, heat loss from the wall to ambient increases, reducing the temperature level of the wall material and hence for the fluid. That results in a much lower value of Gr_m for the same wall thickness. However, warmer ambient condition provides larger value of Gr_m, as was observed in earlier cases. Increased wall thickness reduces the system effectiveness (ε), as can be seen from Fig. 12, because of larger external surface area.

Because of the dominant nature of convective heat transfer over wall conduction, wall material is not expected to have much influence on steady-state behaviour of the system. Wall-to-fluid heat transfer is determined by the associated heat transfer coefficient (H_{in}), which, in turn, is a function of fluid properties and flow kinematics, and hence strong convective interaction between fluid and wall nullifies the effect of wall conduction. However, with increase in wall thickness, enhanced conduction effect attempts to neutralize the temperature gradient between hot and cold sections. Fig. 13 shows the wall temperature profiles for three different materials, namely, AISI 302 steel ($\lambda_w = 15.1$ W m^{-1} K^{-1}), copper ($\lambda_w = 401$ W m^{-1} K^{-1}) and aluminum ($\lambda_w = 237$ W m^{-1} K^{-1}). For smaller wall thickness, there is hardly any distinguishable difference between the corresponding profiles. However, for larger wall thickness, effect of wall conductivity is quite evident, particularly, on either side of the heat-exchanging sections. Use of copper as wall material provides a much smoother temperature profile, because of higher thermal conductivity of copper, thereby emphasizing the increased conduction effects.

4. Conclusions

Considering the wide applicability of NCLs and possible hazardous effects of wall heat loss [23], a numerical model has been developed to investigate the influence of various geometric parameters on the steady-state performance of a single-phase NCL. A rectangular loop has been considered with constant power input at bottom horizontal arm and convective cooling through a parallel-flow heat exchanger around top horizontal arm. Vertical arms are considered to be subjected to heat loss to ambient. Conservation equations were non-dimensionalized using suitable dimensionless quantities and the resulting set of coupled equations was solved following a pseudo-steady approach. Control volume techniques have been used to convert PDEs to algebraic equations. Obtained temperature profiles for wall material, loop fluid and coolant stream, and steady-state mass flux of loop fluid completely describe the behaviour of the system. Numerically predicted values show good agreement with a corresponding experimental data [29], particularly in the turbulent regime.

It was observed that when the steady-state Gr_m is a function of some geometric parameters such as diameter or height, along with average volume expansion coefficient, the concerned geometric parameter is the dominating factor and the profile of Gr_m and Re follows identical trends. However, when Gr_m is a function of β_{av} alone, then they follow reciprocal relationship, as was found in Section 3.4. Major findings can be summarized as the followings.

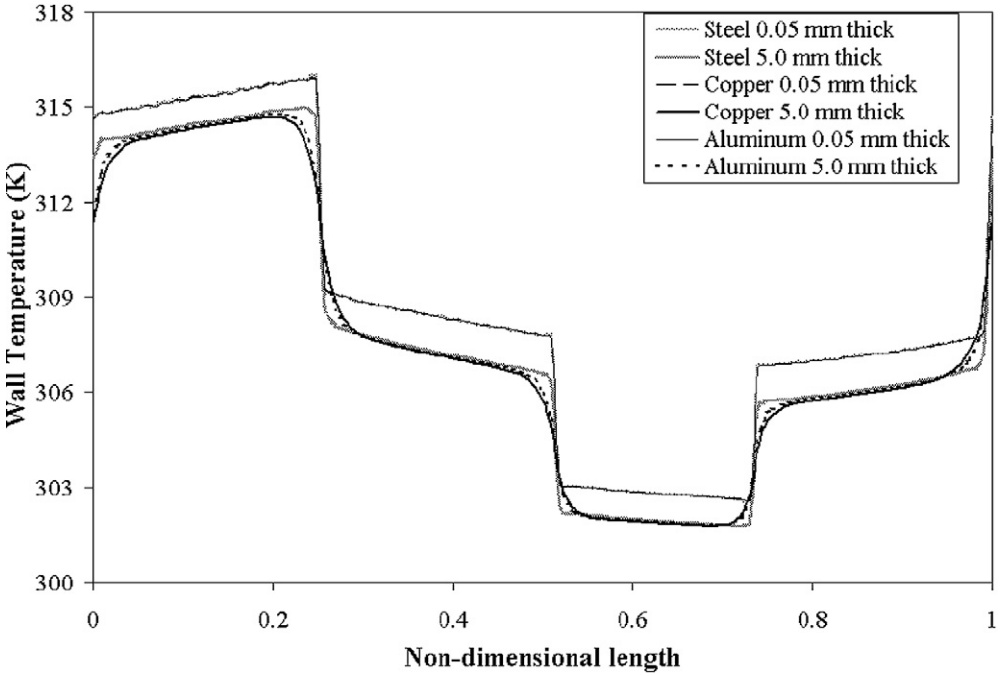

Fig. 13. Effect of wall material on wall temperature profile for 500 W power input.

(1) With increase in loop height, steady-state Grashof No. (Gr_m), being a strong function of height, increases linearly for no-heat-loss case and so does the corresponding Reynolds No. (Re_{ss}). However, when heat loss is included, due to lower temperature levels of wall and loop fluid, sharp decrease in β_{av} produces a flatter profile of Gr_m.
(2) Taller loops provide additional exposed surface causing increase in heat loss to ambient. That reduces loop effectiveness and coolant outlet temperature. In fact, for taller loops under cold ambient condition, it is possible to have negative effectiveness, i.e., net decrease in coolant temperature across the cooler.
(3) Increase in non-insulated horizontal sections increases heat loss, and so the loop yields lower Gr_m and rapid decrease in effectiveness.
(4) Decrease in heater length decreases Gr_m and increases loop mass flux and Re_{ss}, because of the reciprocal relationship. Sharp changes in the gradients of these parameters have been observed beyond certain values of heater length, depending on average fluid temperature. Resulting higher value of wall-to-fluid heat transfer coefficient and associated temperature differential causes the wall temperature profiles to reverse the trend beyond some point.
(5) Increase in inner diameter increases the loop flow rate and Gr_m, but causes a rapid decrease in loop effectiveness, as has been reported earlier by the authors [23].
(6) Higher wall thickness increases wall heat conduction leading to a small reduction in fluid temperature level and hence a small decrease in Gr_m. Larger outer diameter causes a small decrease in loop effectiveness. However, use of materials with higher thermal conductivity and larger wall thickness produces smoother temperature profile for wall material, especially on either side of the heat-exchanging sections.

From an overall perspective, it is found to be advantageous to have a loop with smaller loop height and smaller diameter to obtain higher effectiveness. However, both of them contribute to reduce the loop flow rate. Heater length should be larger to enhance wall-to-fluid heat transfer and also to avoid rapid changes in flow rate during any fluctuation. Uninsulated sections in the horizontal arms serve no purpose, other than increasing heat loss and should be kept to a minimum. Use of highly conductive wall material helps in avoiding larger temperature gradient inside the fluid and slightly increases loop effectiveness due to enhanced heat transfer on coolant side. However, gain in effectiveness is very small and practical issues such as cost and availability should be given priority while selecting the wall material.

Acknowledgement

The financial support extended by the Reactor Engineering Division of Bhabha Atomic Research Centre (BARC), Mumbai, India is gratefully acknowledged.

References

[1] D. Japikse, Advances in thermosyphon technology, in: T.F. Irvine Jr., J.P. Hartnett (Eds.), Advances in Heat Transfer, vol. 9, Academic Press, New York, 1973, pp. 1–111.
[2] Y. Zvirin, A review of natural circulation loops in pressurized water reactors and other systems, Nucl. Eng. Design 67 (1981) 203–225.
[3] A. Metrol, R. Greif, A review of natural circulation loops, in: S. Kakac, W. Aung, R. Viskanta (Eds.), Natural Convection: Fundamentals & Applications, Hemisphere, New York, 1985, pp. 1033–1071.

[4] J.B. Keller, Periodic oscillations in a model of thermal convection, J. Fluid Mech. 26 (1966) 599–606.
[5] P. Welander, On the oscillatory instability of a differentially heated fluid loop, J. Fluid Mech. 29 (1967) 17–30.
[6] Y. Zvirin, R. Greif, Transient behavior of natural circulation loops: Two vertical branches with point heat source and sink, Int. J. Heat Mass Transfer 22 (4) (1979) 499–504.
[7] H.F. Creveling, J.F. De Paz, J.Y. Baladi, R.J. Schoenhals, Stability characteristics of a single-phase free convection loop, J. Fluid Mech. 67 (1975) 65–84.
[8] P.S. Damerell, R.J. Schoenhals, Flow in a toroidal thermosyphon with angular displacement of heated and cooled sections, ASME J. Heat Transfer 101 (1979) 672–676.
[9] J.E. Hart, A new analysis of the closed loop thermosyphon, Int. J. Heat Mass Transfer 27 (1) (1984) 125–136.
[10] M. Sen, E. Ramos, C. Trevino, The toroidal thermosyphon with known heat flux, Int. J. Heat Mass Transfer 28 (1) (1985) 219–233.
[11] H.H. Bau, K.E. Torrance, Transient and steady behaviour of an open symmetrically heated free convection loop, Int. J. Heat Mass Transfer 24 (4) (1981) 597–609.
[12] Y. Zvirin, P.R. Jeuck III, C.W. Sullivan, R.B. Duffey, Experimental and analytical investigation of a natural circulation system with parallel loops, ASME J. Heat Transfer 103 (1981) 645–652.
[13] P.K. Vijayan, A.W. Date, Experimental and theoretical investigations on the steady-state and transient behaviour of a thermosyphon with throughflow in a figure-of-eight loop, Int. J. Heat Mass Transfer 33 (11) (1990) 2479–2489.
[14] M.A. Bernier, B.R. Baliga, A 1-d/2-d model and experimental results for closed loop thermosyphons with vertical heat transfer sections, Int. J. Heat Mass Transfer 35 (11) (1992) 2969–2982.
[15] A.K. Nayak, P.K. Vijayan, D. Saha, V. Venkat Raj, Mathematical modelling of the stability of a natural circulation loop, Math. Comput. Model. 22 (9) (1995) 77–87.
[16] P.K. Vijayan, H. Austregesilo, Scaling laws for single-phase natural circulation loops, Nucl. Eng. Design 152 (1994) 331–347.
[17] P.K. Vijayan, H. Austregesilo, V. Teschendroff, Simulation of the unstable oscillatory behavior of single-phase natural circulation with repetitive flow reversals in a rectangular loop using computer code ATHLET, Nucl. Eng. Design 155 (1995) 623–641.
[18] P.K. Vijayan, S.K. Mehta, A.W. Date, On the steady-state performance of natural circulation loops, Int. J. Heat Mass Transfer 34 (9) (1991) 2219–2230.
[19] N.M. Rao, M. Mishra, B. Maiti, P.K. Das, Effect of end heat exchanger parameters on the performance of a natural circulation loop, Int. Comm. Heat Mass Transfer 29 (4) (2002) 509–518.
[20] N.M. Rao, Investigations on buoyancy induced circulation loops, Ph.D. thesis, Indian Institute of Technology, Kharagpur, 2002.
[21] P.K. Vijayan, Experimental observations on the general trends of the steady-state and stability behaviour of single-phase natural circulation loops, Nucl. Eng. Design 215 (2002) 139–152.
[22] Y.Y. Jiang, M. Shoji, Flow stability in a natural circulation loop: influence of wall thermal conductivity, Nucl. Eng. Design 222 (2003) 16–28.
[23] D.N. Basu, S. Bhattacharyya, P.K. Das, Effect of heat loss to ambient on steady-state behaviour of a single-phase natural circulation loop, Appl. Thermal Eng. 27 (2007) 1432–1444.
[24] V. Gnielinski, Equations for calculating heat transfer in single tube rows and banks of tubes in transverse direction, Int. Chem. Eng. 19 (3) (1979) 380–391.
[25] B.T. Nijaguna, Thermal Sciences/Engineering Data Book, Allied Publishers Limited, New Delhi, 1992, pp. K-13.
[26] S.W. Churchill, H.H.S. Chu, Correlating equations for laminar and turbulent free convection from vertical plate, Int. J. Heat Mass Transfer 18 (11) (1975) 1323–1329.
[27] W. Wagner, J.R. Copper, A. Dittmann, J. Kijima, H.J. Kretzschmar, A. Kruse, R. Mares, K. Oguchi, H. Sato, I. Stocker, O. Sifner, Y. Takaishi, I. Tanishita, J. Trubenbach, Th. Willkommen, The IAPWS industrial formulation 1997 for the thermodynamic properties of water and steam, ASME J. Eng. Gas Turbine Power 122 (2002) 150–182.
[28] F.P. Incropera, D.P. Dewitt, Fundamentals of Heat and Mass Transfer, fifth ed., John Wiley & Sons, Singapore, 2002.
[29] S.K. Mousavian, M. Misale, F. D'Auria, M.A. Salehi, Transient and stability analysis in single-phase natural circulation, Ann. Nucl. Energy 31 (2004) 1177–1198.
[30] S.W. Churchill, H.H.S. Chu, Correlating equations for laminar and turbulent free convection from a horizontal cylinder, Int. J. Heat Mass Transfer 18 (9) (1975) 1049–1053.